

Real versus artifactual symmetry-breaking effects in Hartree–Fock, density-functional, and coupled-cluster methods

Cite as: J. Chem. Phys. **120**, 7298 (2004); <https://doi.org/10.1063/1.1687336>

Submitted: 12 November 2003 . Accepted: 28 January 2004 . Published Online: 05 April 2004

Nicholas J. Russ, T. Daniel Crawford, and Gregory S. Tschumper



View Online



Export Citation

ARTICLES YOU MAY BE INTERESTED IN

[Gaussian basis sets for use in correlated molecular calculations. I. The atoms boron through neon and hydrogen](#)

The Journal of Chemical Physics **90**, 1007 (1989); <https://doi.org/10.1063/1.456153>

[Density-functional thermochemistry. III. The role of exact exchange](#)

The Journal of Chemical Physics **98**, 5648 (1993); <https://doi.org/10.1063/1.464913>

[The equation of motion coupled-cluster method. A systematic biorthogonal approach to molecular excitation energies, transition probabilities, and excited state properties](#)

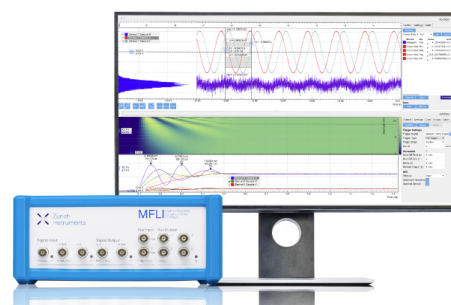
The Journal of Chemical Physics **98**, 7029 (1993); <https://doi.org/10.1063/1.464746>

Challenge us.

What are your needs for periodic signal detection?



Zurich
Instruments



Real versus artifactual symmetry-breaking effects in Hartree–Fock, density-functional, and coupled-cluster methods

Nicholas J. Russ and T. Daniel Crawford^{a)}

Department of Chemistry, Virginia Tech, Blacksburg, Virginia 24061

Gregory S. Tschumper

Department of Chemistry and Biochemistry, University of Mississippi, University, Mississippi 38677

(Received 12 November 2003; accepted 28 January 2004)

We have examined the relative abilities of Hartree–Fock, density-functional theory (DFT), and coupled-cluster theory in describing second-order (pseudo) Jahn–Teller (SOJT) effects, perhaps the most commonly encountered form of symmetry breaking in polyatomic molecules. As test cases, we have considered two prototypical systems: the ${}^2\Sigma_u^+$ states of $D_{\infty h}$ BNB and C_3^+ for which interaction with a low-lying ${}^2\Sigma_g^+$ excited state leads to symmetry breaking of the nuclear framework. We find that the Hartree–Fock and B3LYP methods correctly reproduce the pole structure of quadratic force constants expected from exact SOJT theory, but that both methods appear to underestimate the strength of the coupling between the electronic states. Although the Tamm–Dancoff (CIS) approximation gives excitation energies with no relationship to the SOJT interaction, the random-phase-approximation (RPA) approach to Hartree–Fock and time-dependent DFT excitation energies predicts state crossings coinciding nearly perfectly with the positions of the force constant poles. On the other hand, the RPA excited-state energies exhibit unphysical curvature near their crossings with the ground (reference) state, a problem arising directly from the mathematical structure of the RPA equations. Coupled-cluster methods appear to accurately predict the strength of the SOJT interactions between the ${}^2\Sigma_u^+$ and ${}^2\Sigma_g^+$ states, assuming that the inclusion of full triple excitations provides a suitable approximation to the exact wave function, and are the only methods examined here which predict symmetry breaking in BNB. However, coupled-cluster methods are plagued by artifactual force constant poles arising from the response of the underlying reference molecular orbitals to the geometric perturbation. Furthermore, the structure of the “true” SOJT force constant poles predicted by coupled-cluster methods, although correctly positioned, has the wrong structure. © 2004 American Institute of Physics. [DOI: 10.1063/1.1687336]

I. INTRODUCTION

Within the field of electronic structure theory, the term “spatial symmetry breaking” is generally applied to two phenomena: (1) the failure of the electronic wave function to transform as an irreducible representation of the molecular point group and (2) the preference of the nuclear framework for a lower-symmetry geometry. The first phenomenon results from the use of approximate wave function models and is purely artifactual in that the *exact* wave function necessarily obeys the symmetry properties of the molecular point group. Although model electronic wave functions are frequently constructed such that they maintain spatial symmetry, such wave functions are not always energetically optimal. The question of whether to relax symmetry constraints to obtain lower-energy, but symmetry-contaminated wave functions was described by Löwdin as the “symmetry dilemma.”¹ The second phenomenon, however, may be either real or artifactual, depending on the quality of the model.² For degenerate electronic states, symmetry breaking in the nuclear framework may result from first-order Jahn–Teller effects (also known as Renner–Teller effects in linear

molecules), while nondegenerate states often encounter second-order (or “pseudo”) Jahn–Teller (SOJT) effects, resulting from interactions between different states.

SOJT interactions, which appear frequently in quantum chemical calculations on radical species, were originally described by Von Neumann and Wigner.³ Within the Born–Oppenheimer approximation, electronic states belonging to different irreducible representations of the molecular point group may intersect at certain totally symmetric nuclear configurations. Displacements along nontotally symmetric nuclear coordinates, however, may lead to mixing of the states if their respective irreducible representations correlate in the reduced-symmetry point group. The effect on the energies of the interacting states is often described in terms of Herzberg–Teller coupling, which, to second order in the nuclear displacements, may be written as⁴

$$E_i^{(2)} = \frac{1}{2} \sum_{\alpha} \langle \Psi_i | \frac{\partial^2 \hat{H}}{\partial Q_{\alpha}^2} | \Psi_i \rangle Q_{\alpha}^2 + \sum_{\alpha} \sum_{k \neq i} \frac{\left| \langle \Psi_i | \left(\frac{\partial \hat{H}}{\partial Q_{\alpha}} \right) | \Psi_k \rangle \right|^2}{E_i - E_k} Q_{\alpha}^2 \quad (1)$$

^{a)}Electronic mail: crawdad@vt.edu

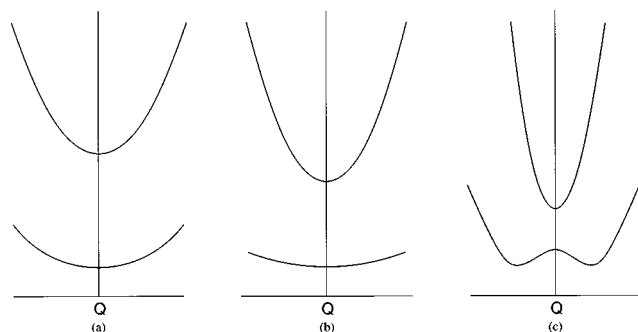


FIG. 1. Schematic depictions of (a) weak, (b) intermediate, and (c) strong second-order Jahn–Teller interactions along a symmetry-breaking coordinate Q .

where Ψ_i and Ψ_k represent the i th and k th (exact) adiabatic states, respectively, of the molecular Hamiltonian \hat{H} , and E_i and E_k are their associated zeroth-order energies. At critical reference coordinates, $Q_\alpha=0$, one or more excited states Ψ_k may become nearly degenerate with the state Ψ_i . As a result, the denominator of the second term above approaches zero and the second-order energy correction exhibits a singularity manifested in the curvature (quadratic and higher-order force constants) of the energy along the coordinate Q_α that induces the mixing between the states. The width of the singularity is governed by the vibronic coupling strength appearing in the numerator of Eq. (1).

Figure 1 illustrates weak, medium, and strong SOJT interactions between two adiabatic states Ψ_i and Ψ_k for the “exact” Born–Oppenheimer case described above. In each plot, Q represents a symmetry-breaking vibrational coordinate, and therefore $Q=0$ corresponds to a high-symmetry molecular geometry. In case (a), the two states are well separated energetically, and little interaction can be observed in the curvature of either state along Q . In case (b), the energetic separation between the states is reduced, leading to concomitantly reduced curvature along Q for the lower state Ψ_i and increased curvature for the upper state Ψ_k —i.e., the states “repel” each other. If the energy difference between the states is further reduced [case (c)], the curvature in Ψ_i becomes negative once the second term in Eq. (1) becomes dominant, leading to a double-well potential along Q and an imaginary vibrational frequency for the corresponding normal mode at $Q=0$. As the two states become exactly degenerate, the force constants in the lower and upper states approach negative and positive infinity, respectively, leading to the well-known double-cone structure (i.e., a conical intersection). After the crossing, the two states reverse their roles in the figure, and each exhibits an overall first-order singularity in its force constants.

One may raise a reasonable objection to the use of Eq. (1) to describe vibronic interactions between nearly degenerate electronic states, because the nondegenerate perturbation theory on which this equation is based will not converge in the region of the potential energy surface (PES) where these states cross. Indeed, the force constant singularities predicted by Eq. (1) will occur even for the exact (full configuration interaction) electronic wave function. A better approach to modeling the interaction might be to use a degenerate pertur-

bation theory expanded around the crossing point. This would require explicit determination of the wave functions for the two (or more) interacting states (which, for approximate methods, are not necessarily directly related to the computed force constants, as we discuss below) and subsequent diagonalization of a corresponding interaction Hamiltonian coupling the states. However, the purpose of the present research is not to develop a robust vibronic coupling model (for an example see Ref. 5), but instead to compare the quality of predictions from low- and high-level electronic structure methods. For this purpose, Eq. (1) is of immense practical value because it provides a relatively simple route for making such comparisons.

The focus of this work is on whether approximate quantum chemical methods adequately reproduce the exact SOJT behavior described above. In particular, we consider the ability of Hartree–Fock, density-functional theory (DFT),⁶ and coupled-cluster methods^{7–10} to describe SOJT effects. We choose as our test cases two prototypical systems: isoelectronic BNB and C_3^+ .

The structure of the BNB molecule has been the focus of several theoretical and experimental investigations.^{11–16} Electron spin resonance (ESR) experiments by Knight *et al.* yielded a $D_{\infty h}$ geometrical structure,¹³ in agreement with earlier theoretical analyses of Martin *et al.*^{14,15} However, subsequent pulsed-laser experiments of Andrews and co-workers provided evidence for both linear and cyclic BNB structures.^{16–18} In 1999, Asmis, Taylor, and Neumark¹¹ published an analysis of the photoelectron spectrum of BNB^- , including extensive theoretical calculations designed to elucidate the SOJT interaction between the ground $2\Sigma_u^+$ state and the lowest excited $2\Sigma_g^+$ state. They found that DFT methods (specifically B3LYP) predicted a $D_{\infty h}$ equilibrium structure, but the corresponding antisymmetric stretching potential failed to reproduce the experimental vibrational progressions. Coupled-cluster methods, on the other hand, predicted a broken-symmetry structure and a double-well potential whose vibrational eigenvalues agreed reasonably well with experiment. However, the zero-point vibrational energy of the mode exceeded the barrier between $C_{\infty v}$ minima, and thus, the experimental data would not allow them to distinguish between such a “quasisymmetric” structure (with dynamical $D_{\infty h}$ symmetry) and a truly symmetric structure with a shallow well along the ν_3 mode. They did note, however, that “the B3LYP model clearly underestimates the extent of Herzberg–Teller [SOJT] coupling.”

Two years later, Gwaltney and Head-Gordon applied high-level coupled-cluster methods to BNB in an attempt to unequivocally characterize the shape of the antisymmetric stretching potential.¹² They showed that many *ab initio* techniques failed due to the presence of molecular orbital Hessian singularities (*vide infra*) and that these obstacles were overcome only when Brueckner-orbital coupled-cluster theory was extended to include full triple excitations. They predicted a $C_{\infty v}$ minimum-energy structure with a difference in B–N bond lengths of 0.09 Å. Furthermore, in agreement with the conclusions of Asmis *et al.*, they determined the $D_{\infty h}$ barrier to lie only 161 cm^{-1} above this minimum, well below the 355- cm^{-1} zero-point vibrational level for ν_3 .

The second prototype considered here is C_3^+ , which is isoelectronic to BNB. In 1987, the first experimental analysis of this molecule was reported by Faibis *et al.* using Coulomb explosion experiments,¹⁹ from which they concluded that the geometrical structure is bent. In a later publication,²⁰ they modified their original interpretation to include the possibility of a “hot” linear structure. Soon afterwards, a surge of theoretical investigations was reported with a range of *ab initio* methods, including configuration interaction,²¹ coupled cluster,^{22–24} quadratic configuration interaction,²⁵ and multi-reference methods.²⁶ All of these reports agreed that a bent C_{2v} structure is indeed the global minimum on the PES, but results were mixed as to the nature of the antisymmetric stretching vibrational mode when C_3^+ was constrained to linear geometries. More recently, Orlova and Goddard reported a DFT study of C_3^+ using B3LYP and BP86 functionals and showed that, while the B3LYP method suffered from apparent orbital instability effects, both DFT methods predicted a real vibrational frequency for the ω_3 antisymmetric stretch.²⁷

The goal of the present work is neither to provide definitive minimum-energy structures nor to accurately simulate the vibrational spectra of BNB and C_3^+ , but instead to analyze the relative abilities of various quantum chemical methods in the description of SOJT effects. Thus we will consider only linear $D_{\infty h}$ geometries, for which the interactions between the two pertinent states $^2\Sigma_u^+$ and $^2\Sigma_g^+$ occur only along the unique antisymmetric stretching coordinate Q_3 . This interaction is manifested in the associated F_{33} quadratic force constant and the corresponding excitation energy.

II. THEORETICAL CONSIDERATIONS

A. Hartree–Fock theory

In the exact SOJT theory described above, the singularity in the quadratic force constant coincides precisely with degeneracy of the interacting electronic states. In other words, the second derivative of the energy depends upon the inverse of a response matrix (the electronic Hamiltonian), such that singularity of this matrix leads to a first-order pole in the force constant. In Hartree–Fock theory, however, this is not the case: quadratic force constants depend instead upon the inverse of the molecular orbital (MO) Hessian, defined as the matrix of second derivatives of the Hartree–Fock energy with respect to nonredundant MO rotation parameters. This matrix arises naturally as part of the coupled perturbed Hartree–Fock (CPHF) equations.^{28–36} The eigenvalues of this Hessian are not excitation energies, but instead represent stability indices of the given (stationary) solution to the Hartree–Fock equations on the orbital rotation hypersurface. Electronic excitation energies in Hartree–Fock theory may be computed as eigenvalues of response matrices defined in a variety of ways, which are intimately related to each other and to the MO Hessian via the nonsymmetric eigenvalue equation^{37,38}

$$\begin{pmatrix} \mathbf{A} & \mathbf{B} \\ -\mathbf{B} & -\mathbf{A} \end{pmatrix} \begin{pmatrix} \mathbf{X} \\ \mathbf{Y} \end{pmatrix} = \Delta E \begin{pmatrix} \mathbf{X} \\ \mathbf{Y} \end{pmatrix}, \quad (2)$$

where

$$\mathbf{A}_{ai,bj} = \langle \Phi_i^a | \hat{H} | \Phi_j^b \rangle = \delta_{ij} \delta_{ab} (f_{aa} - f_{ii}) + \langle ja || bi \rangle \quad (3)$$

and

$$\mathbf{B}_{ai,bj} = \langle \Phi_0 | \hat{H} | \Phi_{ij}^{ab} \rangle = \langle ij || ab \rangle. \quad (4)$$

In the above notation, i, j (a, b) denote occupied (unoccupied) molecular (spin) orbitals, f_{pq} are Fock matrix elements, $\langle pq || rs \rangle$ are antisymmetrized two-electron MO integrals in Dirac’s notation, and $|\Phi_0\rangle$, $|\Phi_i^a\rangle$, and $|\Phi_{ij}^{ab}\rangle$ are the Hartree–Fock determinant, singly excited determinants, and doubly excited determinants, respectively. The vectors \mathbf{X} and \mathbf{Y} parametrize, respectively, single-excitation and -deexcitation components of the excited-state wave functions. Solution of the above equations for the excitation energies ΔE corresponds to the random-phase approximation (RPA),^{37,38} whereas the reduced equation involving only \mathbf{A} in the upper block corresponds to the CIS or Tamm–Dancoff method.³⁹ The MO Hessian, on the other hand, may be written as the sum of the \mathbf{A} and \mathbf{B} matrices. The eigenvalues of the MO Hessian will thus not correspond to excitation energies, except in the (unphysical) limit that the \mathbf{B} matrix is zero.

B. Density-functional theory

The formal underpinnings of DFT and Hartree–Fock descriptions of SOJT are related by virtue of the close connection between the Kohn–Sham and Hartree–Fock equations. Indeed, just as for Hartree–Fock, DFT force constants are not directly dependent on the excitation-energy response matrices of time-dependent DFT (TDDFT), but on a Kohn–Sham orbital Hessian analogous to its Hartree–Fock counterpart. Furthermore, the TDDFT equations may be written in exactly the same RPA form as Eq. (2) above, but with modified definitions of the component matrices:^{40,41}

$$\mathbf{A}_{ai,bj} = \delta_{ij} \delta_{ab} (f_{aa} - f_{ii}) + \langle ja || bi \rangle - C \langle ja || ib \rangle + (1 - C) \langle ja || bi \rangle_{xc} \quad (5)$$

and

$$\mathbf{B}_{ai,bj} = \langle ij || ab \rangle - C \langle ij || ba \rangle + (1 - C) \langle ij || ab \rangle_{xc}, \quad (6)$$

where the indices now denote Kohn–Sham molecular (spin) orbitals, the subscript “xc” indicates integrals over the exchange–correlation operator, and $C \leq 1$ is a parameter controlling the mixing of Hartree–Fock exchange (e.g., $C = 1$ for the original RPA-like equations and $C = 0$ for pure, gradient-corrected functionals). Just as for Hartree–Fock theory, choosing $\mathbf{B} = 0$ leads to a DFT version of the Tamm–Dancoff approximation, and the Kohn–Sham orbital Hessian is obtained as the sum of \mathbf{A} and \mathbf{B} .⁴² We note that, although this research focuses primarily on the popular B3LYP density functional, recent work by Sherrill, Lee, and Head-Gordon⁴³ and by Cohen and Sherrill⁴⁴ provides an analysis of the ability of several density functionals to avoid symmetry-breaking problems in a number of prototypical cases.

C. Coupled-cluster theory

Although coupled-cluster theory has been largely successful in the last 15 years in providing high-accuracy pre-

dictions of a variety of molecular properties⁹—including vibrational frequencies and excitation energies—its efficacy in reproducing correct SOJT behavior has not been well tested. As Stanton recently pointed out in a thorough theoretical analysis of SOJT interactions,⁴ coupled-cluster quadratic force constants exhibit two classes of singularities: one associated with the underlying molecular orbitals and one associated with the correlated wave function parameters. The first, which are sometimes referred to as “CPHF poles,” were first considered in detail for coupled-cluster and other correlated methods by Crawford *et al.*⁴⁵ They showed that, because the coupled-cluster force constant expression depends quadratically on the derivatives (response) of the orbital rotation parameters to nuclear displacements and these derivatives, in turn, depend on the inverse of the MO Hessian (via the CPHF equations, as noted earlier), coupled-cluster force constants necessarily exhibit a second-order pole (dramatically referred to as a “volcano”) in regions where the MO Hessian becomes singular. Such poles are, in a sense, simply artifacts of using MOs that are not variationally optimal at the correlated level of theory. Crawford *et al.* further reported the observation for selected test cases that, for infinite-order methods such as CCSD, these poles tend to be relatively narrow, but for perturbed methods such as CCSD(T), the volcano often widens, indicating that the force constants are artifactually influenced over a larger region of the PES. It is also worth noting that, although for some years Brueckner methods^{46–49} were considered a cure-all for such CPHF poles (and artificial symmetry-breaking problems in general),^{50–53} more recent results indicate that Brueckner-coupled-cluster methods may fail, possibly for *overestimation* of SOJT interactions.⁵⁴

The second type of singularity occurs as a result of the response of the correlated wave function amplitudes to the nuclear perturbation. As Stanton demonstrated, the diagonal coupled cluster quadratic force constant with respect to a coordinate Q may be written as⁴

$$f_{QQ} = \langle \tilde{\Psi}_{\text{CC}} | \frac{\partial^2 \hat{H}}{\partial Q^2} | \Psi_{\text{CC}} \rangle + 2 \sum_k \frac{\langle \tilde{\Psi}_{\text{CC}} | \partial \hat{H} / \partial Q | \Psi_{\text{EOM}}^k \rangle \langle \tilde{\Psi}_{\text{EOM}}^k | \partial \hat{H} / \partial Q | \Psi_{\text{CC}} \rangle}{E - E_k} + \langle \Phi_0 | \hat{L} \bar{H} | \mathbf{q} \rangle \langle \mathbf{q} | \frac{\partial \hat{T}}{\partial Q} \frac{\partial \hat{T}}{\partial Q} | \Phi_0 \rangle, \quad (7)$$

where $|\Psi_{\text{CC}}\rangle$ and $\langle \tilde{\Psi}_{\text{CC}}|$ are the right- and left-hand ground-state coupled-cluster wave functions, $|\Psi_{\text{EOM}}^k\rangle$ and $\langle \tilde{\Psi}_{\text{EOM}}^k|$ are the right- and left-hand equation-of-motion (EOM) coupled-cluster (CC) wave functions for the k th excited state (with associated energy E_k), $|\Phi_0\rangle$ is the Hartree–Fock reference determinant, \hat{T} is the ground-state cluster operator, \bar{H} is the similarity-transformed electronic Hamiltonian $e^{-\hat{T}} \hat{H} e^{\hat{T}}$, \hat{L} is the left-hand, ground-state cluster operator, and the $|\mathbf{q}\rangle$ functions represent excited determinants outside the space generated by $\hat{T}|\Phi_0\rangle$ (e.g., for CCSD $|\mathbf{q}\rangle$ includes triples and higher).

Comparison of Eqs. (1) and (7) reveals correspondence between all but the last term above, which depends quadratically on the response of the cluster amplitudes to the nuclear perturbation. Stanton showed that, in the case that the interacting excited state is a pure single excitation, this term disappears and coupled-cluster theory should reproduce the “true” SOJT behavior of Eq. (1). Of course, some double-excitation (correlation) character naturally arises for all realistic cases, leading to a second-order force constant pole structure. However, although the order of the pole is incorrect as compared to Eq. (1), its position and, in many cases, its width are close to that expected in an exact theory due to (1) the correct dependence of the second term of Eq. (7) on the EOM-CC excitation energies (unlike Hartree–Fock or DFT, whose corresponding expressions depend instead on orbital stability eigenvalues, as noted above) and (2) the fact that these excitation energies generally compare well to full configuration interaction energies.

III. COMPUTATIONAL DETAILS

Optimized geometries and harmonic vibrational frequencies for $D_{\infty h}$ BNB and C_3^+ were computed at a variety of levels of theory. The *ab initio* methods included spin-unrestricted Hartree–Fock (UHF), second-order perturbation theory [MBPT(2)], approximate fourth-order perturbation theory [SDQ-MBPT(4)], coupled-cluster singles and doubles (CCSD),^{55,56} CCSD plus a perturbative estimate of connected triples [CCSD(T)],^{57,58} full coupled-cluster singles, doubles, and triples (CCSDT),^{59–61} and the equation-of-motion CCSD method for ionized states (EOMIP-CCSD).^{61–65} The density functional theory (DFT) approaches included the generalized gradient approximation (GGA) method pairing Becke’s 1988 exchange functional⁶⁶ with the Lee–Yang–Parr correlation functional⁶⁷ (BLYP) as well as the hybrid B3LYP method, which uses Becke’s three-parameter exchange functional⁶⁸ and mixes in Hartree–Fock exchange. Optimized geometries were computed via analytic energy gradients⁶⁹ and harmonic vibrational frequencies via analytic energy second derivatives^{70–72} with all methods except EOMIP-CCSD, for which finite differences of analytic gradients were used,⁶⁵ and with CCSDT, for which finite differences of energies were used.

In addition, linear-response excitation energies and orbital stability eigenvalues were computed for the ${}^2\Sigma_u^+ \rightarrow {}^2\Sigma_g^+$ transition at the following levels of theory: configuration interaction singles (CIS),³⁹ the random phase approximation (RPA),^{37,38} time-dependent-DFT (TDDFT),⁷³ and equation-of-motion-CCSD (EOM-CCSD).⁷⁴ All calculations were performed using the split-valence 6-31G* basis set.⁷⁵ All electrons were correlated in all calculations. The ACESII (Ref. 76) package was used for coupled-cluster and MBPT(n), GAUSSIAN98 (Ref. 77) was used for BLYP and B3LYP, and PS13.2 (Ref. 78) was used for RPA. It should be noted that the results reported here hold also for larger basis sets, e.g., cc-pVTZ,⁷⁹ but we choose to report those only for the 6-31G* basis because full CCSDT calculations were not possible beyond this level.

TABLE I. Energies (E_h), optimized bond lengths (\AA), and harmonic vibrational frequencies (cm^{-1}) for $D_{\infty h}$ ${}^2\Sigma_u^+$ BNB and C_3^+ at several levels of theory computed with a 6-31G* basis set.

	${}^2\Sigma_u^+$ BNB								
	UHF	MBPT(2)	SDQ-MBPT(4)	BLYP	B3LYP	EOMIP-CCSD	CCSD	CCSD(T)	CCSDT
Energy	-103.67388	-103.98456	-103.99917	-104.29210	-104.31599	-103.99968	-103.99918	-104.02225	-104.02308
$r(\text{B-N})$	1.309	1.328	1.326	1.330	1.320	1.324	1.325	1.332	1.332
$\omega_1(\sigma_g^+)$	1245	1182	1181	1156	1192	1192	1186	1161	—
$\omega_2(\pi_u)$	83	153	133	163	158	137	115	134	—
$\omega_3(\sigma_u^+)$	2271	2392	2181	1560	1328	1062 <i>i</i>	1763 <i>i</i>	1566 <i>i</i>	1018 <i>i</i>
	${}^2\Sigma_u^+$ C_3^+								
	UHF	MBPT(2)	SDQ-MBPT(4)	BLYP	B3LYP	EOMIP-CCSD	CCSD	CCSD(T)	CCSDT
Energy	-112.89324	-113.31018	-113.30532	-113.60407	-113.60515	-113.29769	-113.28911	-113.33488	-113.33184
$r(\text{C-C})$	1.282	1.304	1.307	1.307	1.296	1.297	1.298	1.313	1.310
$\omega_1(\sigma_g^+)$	1301	1253	1211	1189	1235	1261	1245	1184	—
$\omega_2(\pi_u)$	145 <i>i</i>	299	240	201	177	149	40	119	—
$\omega_3(\sigma_u^+)$	2496	2917	1857	1512	5589	619 <i>i</i>	2936 <i>i</i>	1662 <i>i</i>	741 <i>i</i>

IV. SOJT INTERACTIONS IN BNB

Table I summarizes the optimized geometries and harmonic vibrational frequencies for the ${}^2\Sigma_u^+$ state of BNB at a number of levels of theory. In general, all methods agree reasonably well on the $\omega_1(\sigma_g^+)$ and $\omega_2(\pi_u)$ vibrational frequencies, but as expected, disagree considerably on the nature of the antisymmetric stretching mode $\omega_3(\sigma_u^+)$: UHF, MBPT(2), and SDQ-MBPT(4) levels predict large real frequencies, BLYP and B3LYP give moderately large frequencies, and all coupled-cluster methods give strong imaginary frequencies, in agreement with the previous calculations of Aismis *et al.*¹¹ and Gwaltney and Head-Gordon.¹² These results and how they relate to SOJT interactions may be understood by considering Figs. 2–6, in which the ω_3 quadratic force constant and ground- and excited-state energies are plotted versus the symmetric B–N stretching coordinate for each method in Table I except the two perturbational methods.

Figure 2 plots UHF force constants and excited-state energies–stability eigenvalues for BNB. The minimum in the ground-state curve occurs at 1.309 \AA , where the correspond-

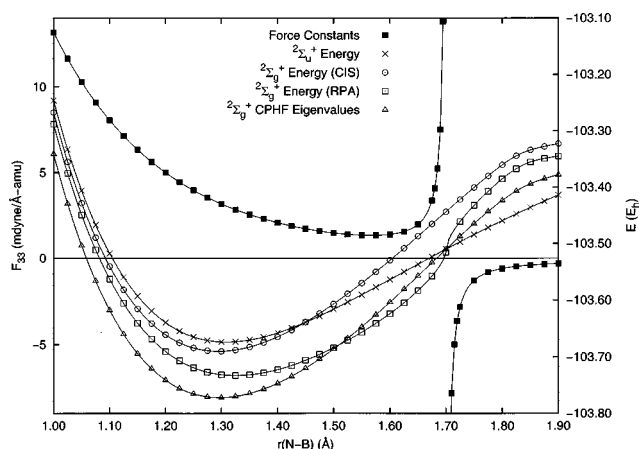


FIG. 2. UHF/6-31G* ${}^2\Sigma_u^+$ quadratic force constants ($\text{mdyne}/\text{\AA} \text{ amu}$), energies (E_h), ${}^2\Sigma_g^+$ CIS and RPA energies (E_h), and orbital stability eigenvalues (E_h) for $D_{\infty h}$ -constrained BNB.

ing quadratic force constant is positive, indicating that the structure is stable with respect to symmetry breaking. We also note the presence of a first-order pole in the force constants at a B–N distance of approximately 1.700 \AA , and as expected from the analysis in Sec. II A above, the CPHF eigenvalues corresponding to σ_u^+/σ_g^+ mixing coincide at exactly this point. For exact SOJT theory, this should also be the crossing point of the ${}^2\Sigma_u^+$ and ${}^2\Sigma_g^+$ states. Furthermore, one would expect the ${}^2\Sigma_u^+$ state to be lower to the left of the singularity and higher to the right. The CIS approach, however, deviates considerably from this expected behavior, and its ${}^2\Sigma_g^+$ energy exhibits a crossing with the ${}^2\Sigma_u^+$ curve at around 1.45 \AA . The RPA method, on the other hand, predicts a correct crossing very near the middle of the force constant singularity. We note, however, that as the RPA excited-state curve approaches the crossing, it exhibits an unphysical curvature.

This curious behavior may be understood by considering the form of the RPA generalized eigenvalue expression in Eq. (2), whose solution normally proceeds by first converting the equation to a reduced-dimension, nonsymmetric eigenvalue expression

$$(\mathbf{A} - \mathbf{B})(\mathbf{A} + \mathbf{B})\mathbf{z} = (\Delta E)^2\mathbf{z}, \quad (8)$$

where \mathbf{A} and \mathbf{B} represent the RPA matrices defined earlier, the excitation vector $\mathbf{z} = \mathbf{X} + \mathbf{Y}$, and ΔE is the excitation energy. If we assume a limiting case of only two orbitals, then \mathbf{A} and \mathbf{B} become scalars, and the excitation energy is

$$\Delta E = (A^2 - B^2)^{1/2}. \quad (9)$$

Differentiating this result with respect to a coordinate Q , we obtain

$$\frac{d\Delta E}{dQ} = \frac{1}{2}(A^2 - B^2)^{-1/2} \left(2A \frac{dA}{dQ} - 2B \frac{dB}{dQ} \right). \quad (10)$$

Thus the slope of ΔE approaches infinity as $\Delta E \rightarrow 0$ —i.e., near a crossing point between the ground- and excited-state energies.⁸⁰ Similar plots have been reported elsewhere in the literature.⁸¹

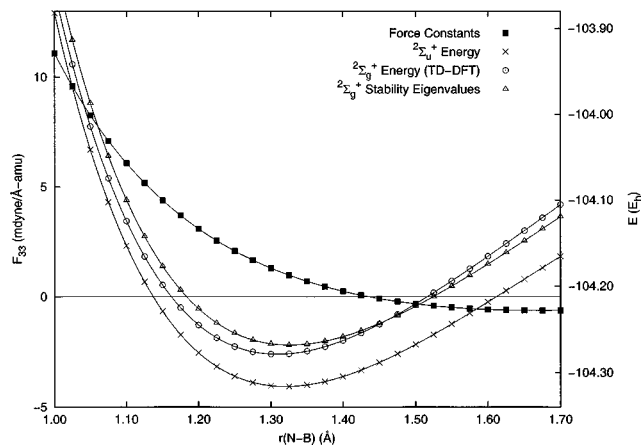


FIG. 3. B3LYP/6-31G* $2\Sigma_u^+$ quadratic force constants (mdyne/Å amu), energies (E_h), and $2\Sigma_g^+$ TD-DFT energies (E_h) for $D_{\infty h}$ -constrained BNB.

Figure 3 plots the analogous force constants and excitation energies for the B3LYP DFT method. The minimum in the ground-state curve occurs at approximately 1.320 Å, where the $2\Sigma_g^+$ state is well separated from the ground state, and the corresponding quadratic force constants are positive, indicating stable $D_{\infty h}$ geometries. No crossing between the states occurs over the domain of B–N distances given here, and the excitation energy at the minimum-energy structure for B3LYP is 1.0 eV. Based on the results of Asmis *et al.*¹¹ and Gwaltney and Head-Gordon,¹² these plots illustrate the underestimation of the SOJT interaction between the states by the B3LYP method.

Figures 4, 5, and 6 plot the same data as above for the CCSD, CCSD(T), and CCSDT methods. Note that the EOM-CC excitation energies governing the SOJT behavior of the CCSD(T) method are exactly the same as those for the CCSD method, due to the perturbative nature of the former. We do not plot the corresponding EOM-CCSDT excitation energies with the CCSDT force constants, however, due to program limitations. Several features of these plots are worthy of note: (1) the EOM-CCSD $2\Sigma_u^+ \rightarrow 2\Sigma_g^+$ excitation energies (ca. 0.6 eV) are smaller than their TDDFT or RPA

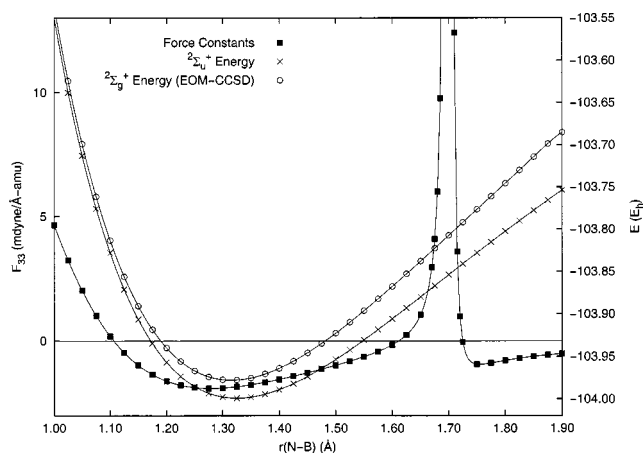


FIG. 4. CCSD/6-31G* $2\Sigma_u^+$ quadratic force constants (mdyne/Å amu), energies (E_h), and $2\Sigma_g^+$ EOM-CCSD energies (E_h) for $D_{\infty h}$ -constrained BNB.

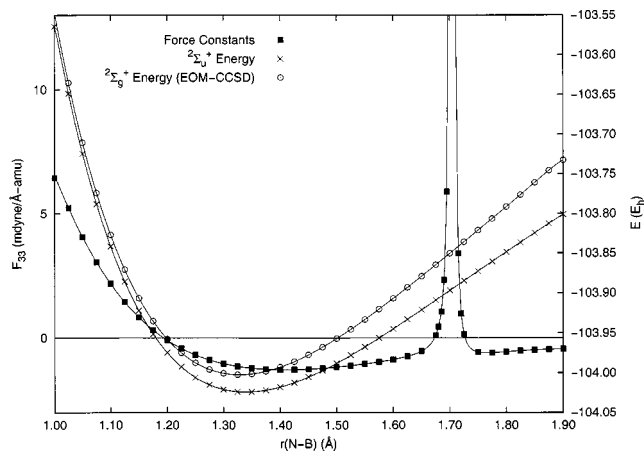


FIG. 5. CCSD(T)/6-31G* $2\Sigma_u^+$ quadratic force constants (mdyne/Å amu), energies (E_h), and $2\Sigma_g^+$ EOM-CCSD energies (E_h) for $D_{\infty h}$ -constrained BNB.

counterparts, and unlike UHF, no crossing between the states occurs; (2) the minimum B–N distance in each is around 1.32 Å, where the corresponding quadratic force constants are negative, indicating SOJT-based symmetry breaking of the molecular framework; (3) all three plots exhibit a second-order pole at approximately 1.70 Å, exactly the point of the first-order pole in the UHF plot (cf. Fig. 2), due to singularity of the MO Hessian, as described by Crawford *et al.*;⁴⁵ (4) somewhat surprisingly, this pole is narrower for CCSD(T) than for CCSD, in contrast to earlier results;⁴⁵ (5) the full CCSDT pole is narrowest, indicating that the force constants are affected over a small domain of B–N distances. Clearly the SOJT interaction as described by coupled-cluster methods is considerably stronger than that given by UHF or DFT methods.

V. SOJT INTERACTIONS IN LINEAR C_3^+

Table I reports optimized geometries and harmonic vibrational frequencies for the $2\Sigma_u^+$ state of C_3^+ at the same levels of theory reported for BNB. Again, all methods agree reasonably well on the $\omega_1(\sigma_g^+)$ and $\omega_2(\pi_u)$ vibrational frequencies, but disagree on the value of the antisymmetric

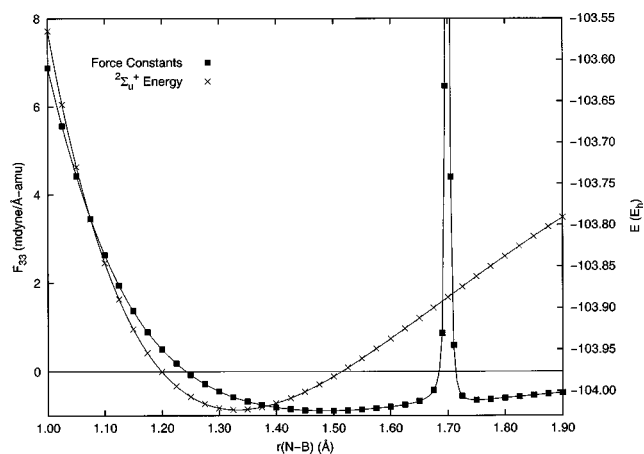


FIG. 6. CCSDT/6-31G* $2\Sigma_u^+$ quadratic force constants (mdyne/Å amu) and energies (E_h) for $D_{\infty h}$ -constrained BNB.

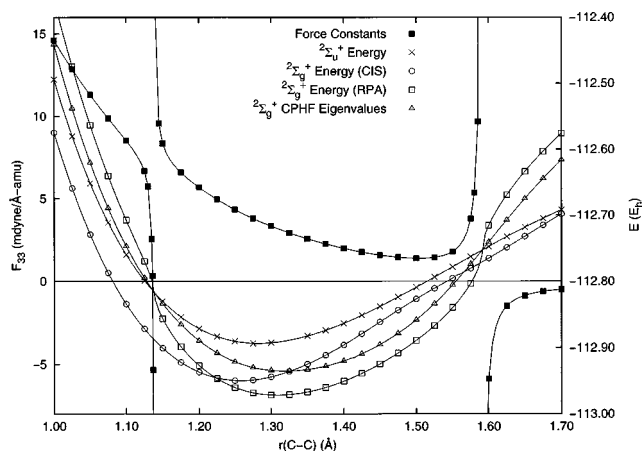


FIG. 7. UHF/6-31G* $2\Sigma_u^+$ quadratic force constants (mdyne/Å amu), energies (E_h), $2\Sigma_g^+$ CIS and RPA energies (E_h), and orbital stability eigenvalues (E_h) for $D_{\infty h}$ -constrained C_3^+ .

stretching mode $\omega_3(\sigma_u^+)$. Just as for BNB, the coupled-cluster methods all give imaginary ω_3 vibrational frequencies, though with much less consistency than before, while all other methods predict a $D_{\infty h}$ minimum. In addition, for C_3^+ the B3LYP method now gives a large, unphysical frequency of 5589 cm^{-1} , in agreement with that reported by Orlova and Goddard²⁷ and indicative of a near-zero eigenvalue of the Kohn–Sham MO Hessian.⁴²

Figure 7 plots UHF quadratic force constants and excitation energy–stability eigenvalues for C_3^+ . The minimum in the ground-state curve occurs at 1.282 Å , corresponding to a positive force constant. However, in this case there are *two* first-order poles present at 1.138 and 1.591 Å , surrounding the $2\Sigma_u^+$ minimum, thus placing the $2\Sigma_g^+$ state *lower* in energy for both CIS and RPA methods. As for BNB, the MO Hessian eigenvalues and RPA “excitation” energies exhibit crossings with the $2\Sigma_u^+$ energy curve in the middle of the singularities, and the RPA energies again show the same unphysical curvature as before in these regions. Once again, the CIS method fails to produce the correct SOJT behavior and, in fact, predicts the $2\Sigma_g^+$ state to lie lower than $2\Sigma_u^+$ for all C–C distances shown.

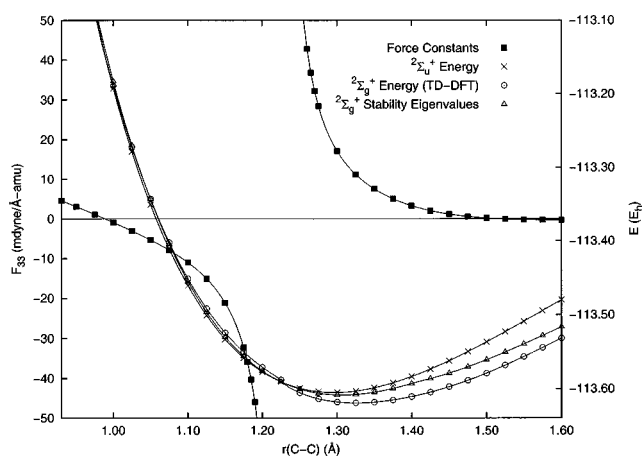


FIG. 8. B3LYP/6-31G* $2\Sigma_u^+$ quadratic force constants (mdyne/Å amu), energies (E_h), and $2\Sigma_g^+$ TD-DFT energies (E_h) for $D_{\infty h}$ -constrained C_3^+ .

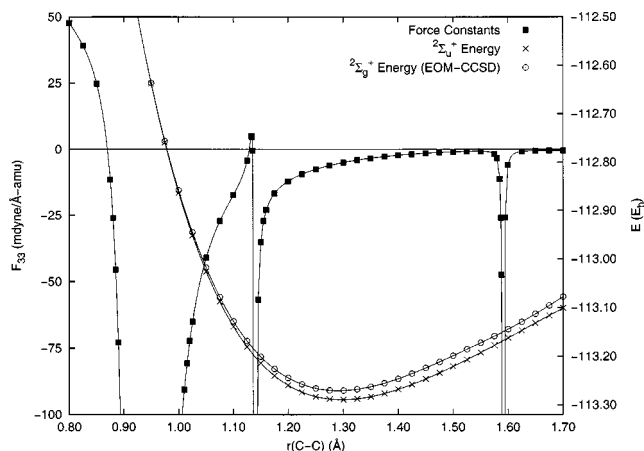


FIG. 9. CCSD/6-31G* $2\Sigma_u^+$ quadratic force constants (mdyne/Å amu), energies (E_h), and $2\Sigma_g^+$ EOM-CCSD energies (E_h) for $D_{\infty h}$ -constrained C_3^+ .

The B3LYP quadratic force constants and associated TDDFT $2\Sigma_g^+$ excited-state energies are shown for C_3^+ in Fig. 8. The most significant difference between C_3^+ and BNB (cf. Fig. 3) is the large first-order pole occurring at $r(\text{C–C})=1.206\text{ Å}$. The $2\Sigma_g^+$ TDDFT energy curve crosses the reference at nearly the same bond length at 1.207 Å and displays the correct ordering of the states as predicted by the force constants. Just as for the RPA, the TDDFT energies show an unphysical curvature as they approach the crossing with the reference curve. This further illustrates the similarities in the formulations of the RPA and TDDFT, and the fundamental reasons for this behavior are similarly explained by Eq. (10) above. However, the TDDFT curves exhibit much less distortion near the crossing than the RPA curves. We further note that the minimum-energy C–C distance of 1.296 Å occurs to the *right* of the singularity, in the region where the $2\Sigma_g^+$ state is the ground state, the opposite from that expected from the BNB results above and from the coupled-cluster C_3^+ results below. At this point, the corresponding quadratic force constants are still significantly influenced by the singularity, leading to the large, real frequency shown in Table I.

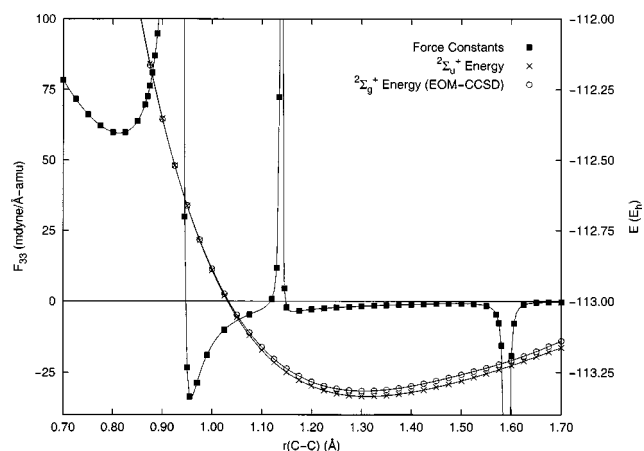


FIG. 10. CCSD(T)/6-31G* $2\Sigma_u^+$ quadratic force constants (mdyne/Å amu), energies (E_h), and $2\Sigma_g^+$ EOM-CCSD energies (E_h) for $D_{\infty h}$ -constrained C_3^+ .

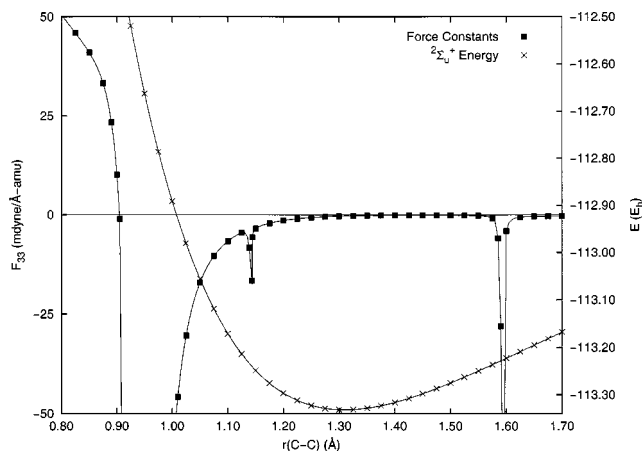


FIG. 11. CCSDT/6-31G* ${}^2\Sigma_u^+$ quadratic force constants (mdyne/Å amu) and energies (E_h) for D_{zh} -constrained C_3^+ .

Finally, Figs. 9, 10, and 11 plot the C_3^+ quadratic force constants and energies for the CCSD, CCSD(T), and CCSDT methods. Unlike BNB, for which only the underlying UHF MO Hessian singularity was present, the C_3^+ plots exhibit *three* singularities: the two at 1.138 and 1.591 Å are artificial and correspond to the UHF singularities considered above; the third at ca. 0.931 Å corresponds to a “correlation” pole [i.e., the “true” SOJT pole as described by Eq. (7)]. The latter occurs exactly at the crossing between the ${}^2\Sigma_u^+$ and ${}^2\Sigma_g^+$ (EOM-CCSD) energies, as expected. Although the correlation pole is second order in all three plots, its structure appears to be perturbed by the nearby UHF singularity at 1.138 Å in the CCSD (9) and CCSD(T) (10) plots. Furthermore, the sign of the correlation pole for CCSD(T) is opposite that of CCSD and CCSDT. This behavior is consistent with that observed by Stanton for the 2B_2 state of NO₂, who noted that “including triple excitation effects *via* CCSD(T) is probably not well advised in studying this class of problems.” Nevertheless, the minimum on the ${}^2\Sigma_u^+$ curve in all three plots occurs between the UHF singularities, and the force constants there do not appear to be dramatically influenced by the artificial poles. The CC methods all predict negative antisymmetric stretching force constants, corresponding to imaginary ω_3 vibrational frequencies and symmetry-broken $C_{\infty v}$ geometries, though the apparent inconsistency among the methods is likely the result of the nearby UHF singularities.

VI. CONCLUSIONS

We have considered the relative abilities of Hartree–Fock, density-functional theory (B3LYP), and coupled-cluster theory in describing SOJT-type symmetry-breaking effects in two prototypical cases, BNB and C_3^+ . Each method has advantages and disadvantages, which we enumerate below:

(1) Hartree–Fock theory describes SOJT interactions through the CPHF equations, which rely not on the CIS or RPA response matrices, but on the MO Hessian, whose eigenvalues are stability indices rather than excitation energies. The corresponding RPA excitation energies do appear nearly

coincident with the force constant singularity, which has the correct first-order structure required by exact SOJT theory. On the other hand, the RPA energies exhibit unphysical curvature near the state crossing, resulting from the mathematical structure of the RPA eigenvalue equations. CIS excitation energies have no connection to the SOJT behavior of Hartree–Fock theory and are therefore useless for such problems.

(2) Density-functional theory (specifically the B3LYP functional) behaves similarly to Hartree–Fock theory in that SOJT force constant singularities are related to the Kohn–Sham MO Hessian rather than true TDDFT excitation energies. Just as for the RPA the TDDFT excited-state energies cross the reference energy very close to the singularity, but the unphysical curvature observed in RPA energies, while also present in the TDDFT curves, is significantly damped relative to its RPA counterpart. Although the B3LYP force constant singularities have the correct first-order pole structure, the BNB and C_3^+ examples suggest that B3LYP underestimates the magnitude of the SOJT coupling.

(3) Coupled-cluster theory appears to correctly describe the strength of the SOJT coupling in these systems, assuming that the full CCSDT method provides a reasonable approximation to the exact (full CI) wave function. However, these methods suffer from the presence of artificial second-order poles arising from the reference MOs. Although these poles are narrow, they can still affect force constants (and other second-order properties) if the optimized structure of interest lies sufficiently close by. Furthermore, the “true” force constant poles predicted by coupled-cluster theory appear to be of the wrong order (second) for the cases considered here, indicating that the ordering of the interacting states cannot be predicted strictly from the signs of the force constants.

ACKNOWLEDGMENTS

This research was supported by a CAREER award from the National Science Foundation (No. CHE-0133174), a New Faculty Award from the Camille and Henry Dreyfus Foundation, and a Cottrell Scholar Award from Research Corporation. The authors thank Professor John F. Stanton (Texas) for helpful discussions.

¹P. O. Löwdin, *Rev. Mod. Phys.* **35**, 496 (1963).

²E. R. Davidson and W. T. Borden, *J. Phys. Chem.* **87**, 4783 (1983).

³J. Von Neumann and E. Wigner, *Z. Phys.* **30**, 467 (1929).

⁴J. Stanton, *J. Chem. Phys.* **115**, 10 382 (2001).

⁵M. Mayer, L. S. Cederbaum, and H. Köppel, *J. Chem. Phys.* **100**, 899 (1994).

⁶R. G. Parr and W. Yang, *Density-Functional Theory of Atoms and Molecules* (Oxford University Press, New York, 1989).

⁷T. D. Crawford and H. F. Schaefer, in *Reviews in Computational Chemistry*, edited by K. B. Lipkowitz and D. B. Boyd (VCH, New York, 2000), Vol. 14, Chap. 2, pp. 33–136.

⁸R. J. Bartlett, in *Modern Electronic Structure Theory*, Vol. 2 of *Advanced Series in Physical Chemistry*, edited by D. R. Yarkony (World Scientific, Singapore, 1995), Chap. 16, pp. 1047–1131.

⁹T. J. Lee and G. E. Scuseria, in *Quantum Mechanical Electronic Structure Calculations with Chemical Accuracy*, edited by S. R. Langhoff (Kluwer Academic, Dordrecht, 1995), pp. 47–108.

¹⁰J. Gauss, in *Encyclopedia of Computational Chemistry*, edited by P. Schleyer (Wiley, New York, 1998).

¹¹K. Asmis, T. Taylor, and D. Neumark, *J. Chem. Phys.* **111**, 8838 (1999).

- ¹²S. Gwaltney and M. Head-Gordon, *Phys. Chem. Chem. Phys.* **3**, 4495 (2001).
- ¹³L. Knight, D. Hill, T. Kirk, and C. Arrington, *J. Phys. Chem.* **96**, 555 (1992).
- ¹⁴J. Martin, J. François, and R. Gijbels, *J. Chem. Phys.* **90**, 6469 (1989).
- ¹⁵J. Martin, J. François, and R. Gijbels, *Chem. Phys. Lett.* **193**, 243 (1992).
- ¹⁶L. Andrews and P. H. T. Burkholder, *J. Chem. Phys.* **98**, 922 (1993).
- ¹⁷C. Thompson, L. Andrews, J. Martin, and J. El-Yazal, *J. Phys. Chem.* **99**, 13 839 (1995).
- ¹⁸C. Thompson and L. Andrews, *J. Am. Chem. Soc.* **117**, 10 125 (1995).
- ¹⁹A. Faibis, E. Kanter, L. Tack, E. Bakke, and B. Zabransky, *J. Phys. Chem.* **91**, 6445 (1987).
- ²⁰Z. Vager and E. Kanter, *J. Phys. Chem.* **93**, 7745 (1989).
- ²¹R. S. Grev, I. L. Alberts, and H. F. Schaefer, *J. Phys. Chem.* **94**, 3379 (1990).
- ²²J. Martin, J. P. François, and R. Gijbels, *J. Chem. Phys.* **93**, 5037 (1990).
- ²³G. E. Scuseria, *Chem. Phys. Lett.* **176**, 27 (1991).
- ²⁴J. D. Watts, J. F. Stanton, and R. J. Bartlett, *Chem. Phys. Lett.* **178**, 471 (1991).
- ²⁵K. Raghavachari, *Chem. Phys. Lett.* **171**, 249 (1990).
- ²⁶P. Taylor, J. Martin, J. François, and R. Gijbels, *J. Phys. Chem.* **95**, 6530 (1991).
- ²⁷G. Orlova and J. Goddard, *Chem. Phys. Lett.* **363**, 486 (2002).
- ²⁸J. Čížek and J. Paldus, *J. Chem. Phys.* **47**, 3976 (1967).
- ²⁹J. Paldus and J. Čížek, *Chem. Phys. Lett.* **3**, 1 (1969).
- ³⁰J. Paldus and J. Čížek, *J. Chem. Phys.* **52**, 2919 (1970).
- ³¹J. Paldus and J. Čížek, *J. Chem. Phys.* **54**, 2293 (1971).
- ³²J. Paldus and J. Čížek, *Can. J. Chem.* **63**, 1803 (1985).
- ³³K. Deguchi, K. Nishikawa, and S. Aono, *J. Chem. Phys.* **75**, 4165 (1981).
- ³⁴W. D. Allen, D. A. Horner, R. L. DeKock, R. B. Remington, and H. F. Schaefer, *Chem. Phys.* **133**, 11 (1989).
- ³⁵Y. Yamaguchi, I. L. Alberts, J. D. Goddard, and H. F. Schaefer, *Chem. Phys.* **147**, 309 (1990).
- ³⁶N. A. Burton, Y. Yamaguchi, I. L. Alberts, and H. F. Schaefer, *J. Chem. Phys.* **95**, 7466 (1991).
- ³⁷D. J. Rowe, *Rev. Mod. Phys.* **40**, 153 (1968).
- ³⁸P. Jørgensen and J. Simons, *Second Quantization-Based Methods in Quantum Chemistry* (Academic, New York, 1981).
- ³⁹J. B. Foresman, M. Head-Gordon, J. A. Pople, and M. J. Frisch, *J. Phys. Chem. A* **96**, 135 (1992).
- ⁴⁰R. Bauernschmitt and R. Ahlrichs, *Chem. Phys. Lett.* **256**, 454 (1996).
- ⁴¹S. Hirata and M. Head-Gordon, *Chem. Phys. Lett.* **302**, 375 (1999).
- ⁴²R. Bauernschmitt and R. Ahlrichs, *J. Chem. Phys.* **104**, 9047 (1996).
- ⁴³C. Sherrill, M. Lee, and M. Head-Gordon, *Chem. Phys. Lett.* **302**, 425 (1999).
- ⁴⁴R. Cohen and C. Sherrill, *J. Chem. Phys.* **114**, 8257 (2001).
- ⁴⁵T. D. Crawford, J. F. Stanton, W. D. Allen, and H. F. Schaefer, *J. Chem. Phys.* **107**, 10 626 (1997).
- ⁴⁶R. K. Nesbet, *Phys. Rev.* **109**, 1632 (1958).
- ⁴⁷R. A. Chiles and C. E. Dykstra, *J. Chem. Phys.* **74**, 4544 (1981).
- ⁴⁸L. Z. Stolarczyk and H. J. Monkhorst, *Int. J. Quantum Chem., Symp.* **18**, 267 (1984).
- ⁴⁹N. C. Handy, J. A. Pople, M. Head-Gordon, K. Raghavachari, and G. W. Trucks, *Chem. Phys. Lett.* **164**, 185 (1989).
- ⁵⁰J. F. Stanton, J. Gauss, and R. J. Bartlett, *J. Chem. Phys.* **97**, 5554 (1992).
- ⁵¹L. A. Barnes and R. Lindh, *Chem. Phys. Lett.* **223**, 207 (1994).
- ⁵²Y. Xie, W. D. Allen, Y. Yamaguchi, and H. F. Schaefer, *J. Chem. Phys.* **104**, 7615 (1996).
- ⁵³T. D. Crawford, J. F. Stanton, P. G. Szalay, and H. F. Schaefer, *J. Chem. Phys.* **107**, 2525 (1997).
- ⁵⁴T. D. Crawford and J. F. Stanton, *J. Chem. Phys.* **112**, 7873 (2000).
- ⁵⁵G. D. Purvis and R. J. Bartlett, *J. Chem. Phys.* **76**, 1910 (1982).
- ⁵⁶M. Rittby and R. J. Bartlett, *J. Phys. Chem.* **92**, 3033 (1988).
- ⁵⁷K. Raghavachari, G. W. Trucks, J. A. Pople, and M. Head-Gordon, *Chem. Phys. Lett.* **157**, 479 (1989).
- ⁵⁸R. J. Bartlett, J. D. Watts, S. A. Kucharski, and J. Noga, *Chem. Phys. Lett.* **165**, 513 (1990); **167**, 609(E) (1990).
- ⁵⁹M. R. Hoffmann and H. F. Schaefer, *Adv. Quantum Chem.* **18**, 207 (1986).
- ⁶⁰J. Noga and R. J. Bartlett, *J. Chem. Phys.* **86**, 7041 (1987).
- ⁶¹J. D. Watts and R. J. Bartlett, *J. Chem. Phys.* **93**, 6104 (1990).
- ⁶²U. Kaldor, *Theor. Chim. Acta* **80**, 427 (1991).
- ⁶³D. Mukhopadhyay, S. Mukhopadhyay, R. Chaudhuri, and D. Mukherjee, *Theor. Chim. Acta* **80**, 441 (1991).
- ⁶⁴C. M. L. Rittby and R. J. Bartlett, *Theor. Chim. Acta* **80**, 469 (1991).
- ⁶⁵J. F. Stanton and J. Gauss, *J. Chem. Phys.* **101**, 8938 (1994).
- ⁶⁶A. D. Becke, *Phys. Rev. A* **38**, 3098 (1988).
- ⁶⁷C. Lee, W. Yang, and R. G. Parr, *Phys. Rev. B* **37**, 785 (1988).
- ⁶⁸A. D. Becke, *J. Chem. Phys.* **98**, 5648 (1993).
- ⁶⁹J. Gauss, J. F. Stanton, and R. J. Bartlett, *J. Chem. Phys.* **95**, 2623 (1991).
- ⁷⁰J. Gauss and J. F. Stanton, *Chem. Phys. Lett.* **276**, 70 (1997).
- ⁷¹J. F. Stanton and J. Gauss, in *Recent Advances in Coupled-Cluster Methods*, edited by R. J. Bartlett (World Scientific, Singapore, 1997), pp. 49–79.
- ⁷²P. G. Szalay, J. Gauss, and J. F. Stanton, *Theor. Chim. Acta* **100**, 5 (1998).
- ⁷³M. E. Casida, in *Recent Advances in Density Functional Methods*, edited by D. P. Chong (World Scientific, Singapore, 1995), Vol. 1.
- ⁷⁴J. F. Stanton and R. J. Bartlett, *J. Chem. Phys.* **98**, 7029 (1993).
- ⁷⁵P. C. Hariharan and J. A. Pople, *Theor. Chim. Acta* **28**, 213 (1973).
- ⁷⁶J. F. Stanton, J. Gauss, J. D. Watts, W. J. Lauderdale, and R. J. Bartlett, computer code ACES II, 1993. The package also contains modified versions of the MOLECULE Gaussian integral program of J. Almlöf and P. R. Taylor, the ABACUS integral derivative program written by T. U. Helgaker, H. J. Aa. Jensen, P. Jørgensen, and P. R. Taylor, and the PROPS property evaluation integral code of P. R. Taylor.
- ⁷⁷M. J. Frisch, G. W. Trucks, H. B. Schlegel *et al.*, GAUSSIAN 98, Gaussian, Inc., Pittsburgh, PA, 1998.
- ⁷⁸T. D. Crawford, C. D. Sherrill, E. F. Valeev *et al.*, computer code PSI 3.2, 2003.
- ⁷⁹T. H. Dunning, *J. Chem. Phys.* **90**, 1007 (1989).
- ⁸⁰It should be noted that, if the reference energy is *higher* than the “excited-state” energy in the RPA calculation, $(\Delta E)^2$ in Eq. (8) will be negative. Thus the RPA values plotted in the figures beyond the crossing point with the ground state are, in fact, imaginary excitation energies.
- ⁸¹T. Helgaker, P. Jørgensen, and J. Olsen, *Molecular Electronic Structure Theory* (Wiley, New York, 2000).